Research Article | Vol. 8, No. 3 / March 2020 / Photonics Research 279

PHOTONICS Research

High-power hybrid GaN-based green laser diodes with ITO cladding layer

Lei Hu,[1,2] Xiaoyu Ren,[1] Jianping Liu,[1,2,*] Aiqin Tian,[1] Lingrong Jiang,[1,2] Siyi Huang,[1] Wei Zhou,[1] Liqun Zhang,[1] and Hui Yang[1,2]

[1]Key Laboratory of Nanodevices and Applications, Suzhou Institute of Nano-Tech and Nano-Bionics, Chinese Academy of Sciences (CAS), Suzhou 215123, China
[2]School of Nano-Tech and Nano-Bionics, University of Science and Technology of China, Hefei 230026, China
*Corresponding author: jpliu2010@sinano.ac.cn

Received 23 October 2019; revised 18 December 2019; accepted 22 December 2019; posted 24 December 2019 (Doc. ID 381262); published 12 February 2020

Green laser diodes (LDs) still perform worst among the visible and near-infrared spectrum range, which is called the "green gap." Poor performance of green LDs is mainly related to the p-type AlGaN cladding layer, which on one hand imposes large thermal budget on InGaN quantum wells (QWs) during epitaxial growth, and on the other hand has poor electrical property especially when low growth temperature has to be used. We demonstrate in this work that a hybrid LD structure with an indium tin oxide (ITO) p-cladding layer can achieve threshold current density as low as 1.6 kA/cm^2, which is only one third of that of the conventional LD structure. The improvement is attributed to two benefits that are enabled by the ITO cladding layer. One is the reduced thermal budget imposed on QWs by reducing p-AlGaN layer thickness, and the other is the increasing hole concentration since a low Al content p-AlGaN cladding layer can be used in hybrid LD structures. Moreover, the slope efficiency is increased by 25% and the operation voltage is reduced by 0.6 V for hybrid green LDs. As a result, a 400 mW high-power green LD has been obtained. These results indicate that a hybrid LD structure can pave the way toward high-performance green LDs. © 2020 Chinese Laser Press

https://doi.org/10.1364/PRJ.381262

1. INTRODUCTION

Laser diodes (LDs) based on III-nitride materials (Al, Ga, In)N extend the wavelength of semiconductor lasers into the visible and ultraviolet spectrum range, and therefore have been attracting great attention in the past years due to their huge applications, such as information storage, laser lighting, laser display, and recently emerging applications for atomic cooling and metal processing [1–15]. However, semiconductor lasers with wavelengths in the green spectrum range from 500 nm to 550 nm still perform worst among the visible and near-infrared spectrum range, which is called the "green gap" [16–20]. Green LDs are very important especially for display application to obtain a wide color gamut. However, the performance of GaN-based green LDs cannot meet the demand of laser display yet and is a bottleneck. This is due to large lattice mismatch and the difference in epitaxial growth temperatures between high-indium-content green InGaN quantum wells (QWs) and the p-AlGaN cladding layer. The growth temperature for green InGaN QWs is around 700°C, while it is 950–1000°C for the p-AlGaN cladding layer, which means a large thermal budget imposed on InGaN QWs during epitaxial growth of the p-AlGaN cladding layer. A large thermal budget leads to serious thermal degradation of green InGaN QWs [21–25]. Moreover, the p-AlGaN cladding layer has poor electrical property, especially when low growth temperature has to be used in the green LD structure. Therefore, these issues related to the p-type AlGaN cladding layer have to be solved to improve the performance of green GaN-based LDs.

In order to avoid these disadvantages associated with the p-AlGaN cladding layer, silver (Ag) metal had been explored as a cladding layer and metal p-electrode in GaN-based violet LDs [26]. However, since the absorption coefficient (α) of Ag is as high as 610,000 cm^{-1} at 410 nm, it will induce a large internal loss of 30 cm^{-1}, and thus the LD performance was not improved although lasing had been achieved under electrical injection. Indium tin oxide (ITO), which is conductive and transparent in the visible spectrum range, has been widely used as an electrode in GaN-based light-emitting diodes. The absorption coefficient of ITO is 2 orders of magnitude lower than that of metal. Meanwhile, the refractive index of ITO is around 2, much lower than that of the p-AlGaN cladding layer, and therefore provides sufficient optical confinement for the laser cavity. ITO can be deposited at around 300°C or lower, and therefore replacing the p-AlGaN cladding layer

with ITO can reduce the high-temperature growth time of the p-AlGaN cladding layer, and thus reduce the thermal budget imposed on green InGaN QWs. Moreover, using ITO as the cladding layer also allows a thinner and lower Al content p-AlGaN cladding layer to be used in hybrid LD structures, meaning the electrical property of the cladding layer, including hole concentration and conductivity, can be enhanced. Therefore, hybrid GaN-based LDs using ITO as the p-cladding layer are promising to improve the performance of GaN-based LDs. There are a few reports about the design and fabrication of hybrid GaN-based LDs using ITO as the cladding layer. However, the performance is only comparable to LDs with conventional structures [27–30].

In this work, we demonstrated that the performance of green LDs can be improved greatly by using the ITO cladding layer and reducing the thickness of the p-AlGaN cladding layer. We first designed the LD structures by simulation in order to reduce the internal loss, which was found to be dependent on the remaining p-AlGaN cladding layer thickness and the absorption coefficient of the ITO layer. GaN-based green LDs with an ITO cladding layer were then fabricated and characterized. It was found that the threshold current density was reduced from 5 kA/cm^2 to 2.5 kA/cm^2 and the slope efficiency was increased from 0.16 W/A to 0.2 W/A by using the ITO cladding layer and reducing the thickness of the p-AlGaN cladding layer. The cause for the improvement was attributed to improved quality of green InGaN QWs due to reduced thermal degradation imposed by the p-AlGaN cladding layer growth. The threshold current density was further reduced to 1.6 kA/cm^2 when the average Al content of the p-AlGaN cladding layer was reduced from 8% to 3.5%. Meanwhile, the operation voltage was also reduced by 0.6 V. By employing the ITO cladding layer, a high-power green LD with an output power of 400 mW at the typical operation current density of 9 kA/cm^2 for GaN-based green LDs has been achieved in this work.

2. LASER DESIGN AND FABRICATION

The transfer matrix method was used to calculate the light field distribution, the internal loss, and the confinement factor (Γ) of our green LD structures [31]. The LD structure is shown in Fig. 1(a). The epitaxial structure consisted of a silicon (Si)-doped n-$Al_{0.07}Ga_{0.93}N$ cladding layer; a Si-doped n-GaN layer; a Si-doped n-$In_{0.04}Ga_{0.96}N$ waveguide layer; two-period unintentional-doped multiple quantum wells; an unintentional-doped $In_{0.03}Ga_{0.97}N$ waveguide layer; a magnesium (Mg)-doped p-$Al_{0.15}Ga_{0.85}N$ electron blocking layer; a Mg-doped p-AlGaN cladding layer with average Al content of 8% and 3.5% and various thicknesses from 150 nm to 500 nm (p-AlGaN/p-GaN superlattice structures with 2.5 nm p-AlGaN and 2.5 nm p-GaN in a period were used in order to reduce its resistivity); a p-InGaN contact layer; and an ITO p-electrode or a palladium (Pd)/platinum (Pt)/gold (Au) metal p-electrode.

The refractive indices of (Al, In)GaN were taken from Ref. [32], and the absorption coefficient was interpolated from Ref. [33]. The absorption coefficients of p-AlGaN and Pd used

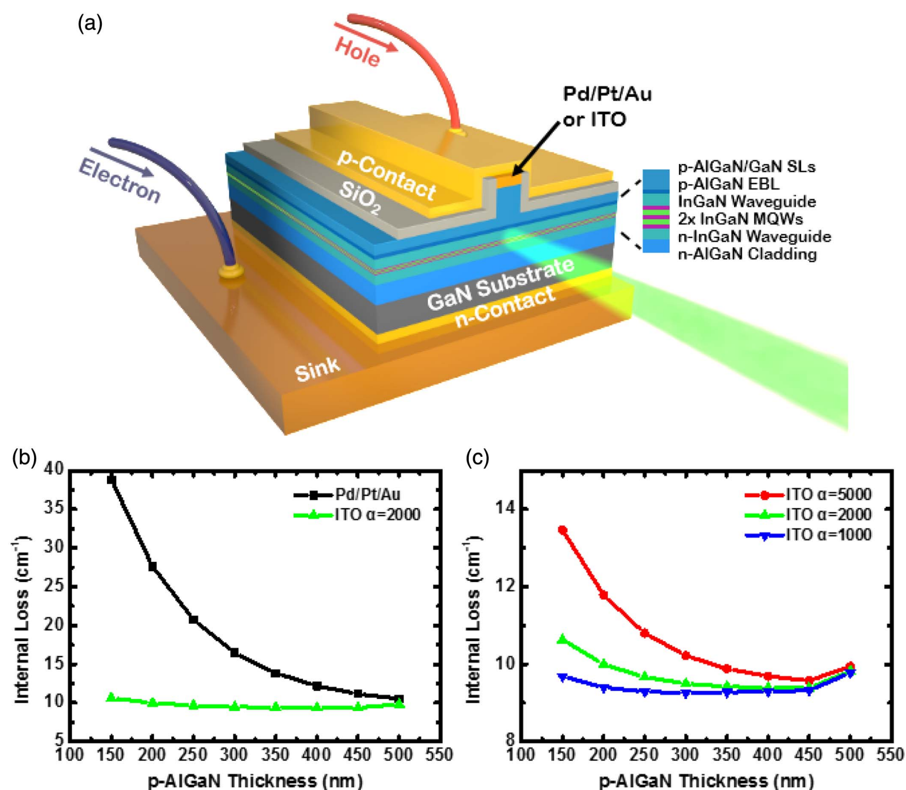

Fig. 1. (a) Structure of the hybrid LD with ITO cladding layer or conventional LD with Pd/Pt/Au electrode. (b) Calculated internal loss of the hybrid LD and conventional LD as a function of p-AlGaN cladding layer thickness. (c) Calculated internal loss of hybrid LDs with various absorption coefficients of ITO layers as a function of p-AlGaN cladding layer thickness.

in the calculation are 50 cm^{-1} and 860,000 cm^{-1}, respectively. As for ITO, three different absorption coefficients of 1000 cm^{-1}, 2000 cm^{-1}, and 5000 cm^{-1} were used in the calculation, which cover general ranges reported for ITO [34–36]. The refractive index of ITO is 1.95 at 520 nm, taken from Ref. [37]. We will show later that the absorption coefficient and the refractive index of ITO deposited by us and used in our LD structure are 2000 cm^{-1} and 1.95 at the wavelength of 520 nm. As for LD structures with the ITO cladding layer, ITO acts as the p-electrode layer and part of the optical cladding layer since it has a much lower refractive index than the p-AlGaN cladding layer, and therefore has better vertical optical confinement. Figure 1(b) shows the relationship between p-AlGaN cladding layer thickness and LD internal loss, which was calculated by summing the product of the confinement factor and the absorption coefficient of each layer. As for the conventional LDs, with the decrease of p-AlGaN cladding layer thickness, the internal loss has a significant increase which results from the rapid increase of light absorption in metal p-electrode since the absorption coefficient of Pd is as large as 860,000 cm^{-1}. On the contrary, as the p-AlGaN cladding layer thickness decreases from 500 nm down to 150 nm in the ITO LD structures, the internal loss even decreases and then increases slightly when the absorption coefficient of ITO is 2000 cm^{-1} and 1000 cm^{-1}, which can be seen in Fig. 1(c), but it is still comparable to that of the conventional LD structure with a 500 nm p-AlGaN cladding layer. Even when the absorption coefficient of ITO is 5000 cm^{-1}, the increase of internal loss is negligible for the LD structure with a 300 nm p-AlGaN cladding layer, and the increase of internal loss is only considerate for the LD structure with a 150 nm p-AlGaN cladding layer, but it is only one third of that of the LD structure with a 150 nm p-AlGaN cladding layer metal electrode.

Three LD epitaxial structures with p-$Al_{0.08}GaN$ cladding layers of 150 nm, 300 nm, and 500 nm, respectively, were grown by metal-organic chemical vapor deposition (MOCVD) on *c*-plane GaN substrates. Inductively coupled plasma dry etching was used to form the ridge waveguide LDs. A 200 nm silicon dioxide layer was deposited as the insulating layer using inductively coupled plasma chemical vapor deposition on both sides of the ridges. A 200 nm ITO layer was then deposited on top of the ridge using electron beam evaporation at a temperature of 300°C for the LD structures with 150 nm, 300 nm, and 500 nm p-AlGaN cladding layers. About 100/500 nm of titanium (Ti)/Au was then deposited on top of ITO as a p-pad and 50/100/50/100 nm of Ti/aluminum (Al)/Ti/Au was deposited on the backside of the wafer to form the n-electrode. For the conventional LD structure with the 500 nm p-AlGaN cladding layer, Pd/Pt/Au was used for the p-electrode. The four LD structures were named as samples S150, S300, S500, and C500, respectively. The LD cavity facets were formed by cleaving among the *m*-plane of the GaN crystal and then deposited dielectric films.

3. RESULTS AND DISCUSSION

Figure 2(a) shows the ellipsometer measurement curves of the ITO layer. By fitting these curves, the absorption coefficient and the refractive index of the ITO layer are determined to be around 2000 cm^{-1} and 1.95 at 520 nm, as shown in Fig. 2(b). These two values have been used in the simulation. The total internal loss of ITO LDs as a function of p-AlGaN cladding layer thickness is shown by the green curve in Fig. 1(b). We use the circular transmission line method to evaluate the contact resistivity between ITO and LD structures. The current versus voltage curves are shown in Fig. 2(c) for

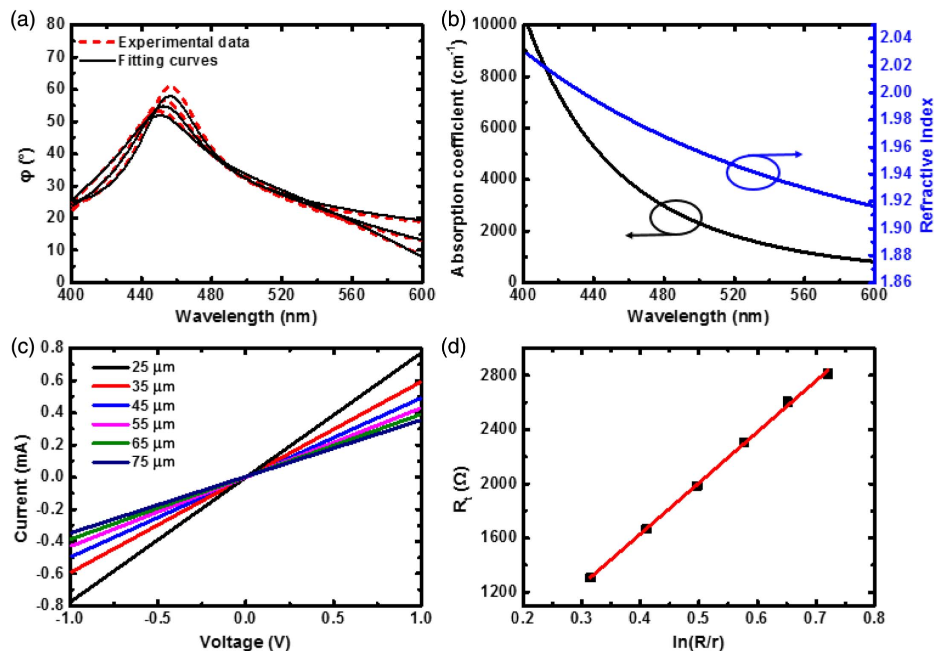

Fig. 2. Optical and electrical characteristics of ITO layer. (a) The ellipsometer measurement curves of the annealed ITO layer. (b) The absorption coefficient and refractive index of the ITO layer fitted by the ellipsometer. (c) Current-voltage curves of circular transmission line method test for various electrode spacing. (d) The specific contact resistivity fitting curve.

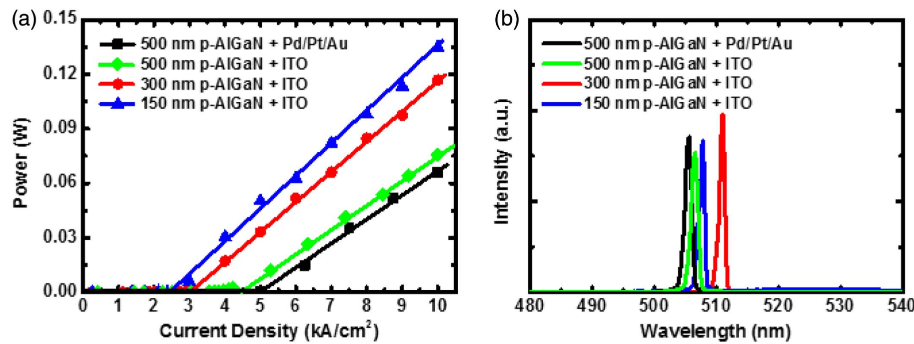

Fig. 3. (a) Power–current (*P–I*) curves of hybrid LDs with ITO cladding layer and conventional LD with Pd/Pt/Au electrode. The P-$Al_{0.08}GaN$ cladding layer thicknesses and electrode are shown in the legends. (b) Lasing spectra of four different kinds of LDs.

various electrode spacing. The specific contact resistivity is calculated to be $3 \times 10^{-4}\ \Omega \cdot cm^2$, as shown in Fig. 2(d) [27,38,39], which is comparable to that of the Pd electrode fabricated by us.

The LD characteristics were measured by probing LD bars under pulse operation at room temperature. The pulse width was 0.4 μs and the repetition rate was 10 kHz to minimize self-heating effects. The typical power–current (*P–I*) curves for ITO LDs with various p-AlGaN cladding layer thicknesses and for conventional LD are shown in Fig. 3(a). The threshold current density of the conventional LD is 5 kA/cm^2, and the slope efficiency is 0.16 W/A. The threshold current density reduces to 4.5 kA/cm^2, 2.9 kA/cm^2, and 2.5 kA/cm^2 for ITO LDs with 500 nm, 300 nm, and 150 nm p-AlGaN cladding layers, while the slope efficiency stays 0.16 W/A and increases to 0.19 W/A and 0.2 W/A, respectively. The lasing spectra of these four LDs are shown in Fig. 3(b). The lasing wavelengths of the ITO LDs with the 500 nm, 300 nm, and 150 nm p-AlGaN cladding layers are 506 nm, 512 nm, and 508 nm, respectively, while it is 505 nm for the conventional LD. The different wavelengths are caused by the growth temperature variation of different MOCVD growth runs.

In order to investigate the reason for the remarkable performance improvement, we measured the electroluminescence (EL) intensity of the LD chips as a function of injected current density and plotted the integrated EL intensity versus injection current density using the double logarithmic scale, as shown in Fig. 4. According to the total recombination equation $R_{total} = An + Bn^2 + Cn^3$, which consists of non-radiative (corresponding to An), radiative (Bn^2), and Auger (Cn^3) recombination processes, such double logarithmic plots can be linearly fitted and the current range that is dominated by non-radiative, radiative, and Auger-type recombination processes can be identified with the slope to be 2, 1, and 2/3, respectively [21,40,41]. The current densities corresponding to the intersection of the linear fitting with slopes of 2 and 1 are 4 A/cm^2, 5 A/cm^2, and 15 A/cm^2 for hybrid LDs with the ITO cladding layer, and 17 A/cm^2 for the conventional LD, respectively, as shown in Fig. 4. This means there are increasing non-radiative recombination centers in the LDs, especially remarkably increasing non-radiative recombination centers in the LDs with the 500 nm p-AlGaN cladding layer. We believe that the increasing non-radiative recombination centers result from the increasing thermal budget due to increasing growth time of the p-AlGaN cladding layer. The difference between ITO LDs with 300 nm and 150 nm p-AlGaN cladding layers is not so large that the threshold current density and slope efficiency of these two samples are similar. The difference between ITO LDs and conventional LDs with the same 500 nm p-AlGaN cladding layer is negligible, which suggests the reduction of LD threshold mainly results from the reduced thermal budget imposed on QWs by decreasing the thickness of the p-AlGaN cladding layer rather than the effects related to the optical and electrical properties of ITO contact.

On the other hand, the changes of total internal loss and confinement factor also affect LD performance. Our simulation shows that the confinement factors of these four samples are almost the same. The simulated total internal loss of sample S300 with 300 nm p-AlGaN cladding layer is 8.2 cm^{-1}, 2.3 cm^{-1} lower than that of conventional LD sample C500, as shown in Fig. 1(c). This reduction of internal loss is not so significant to account for the reduction of the threshold current density and the increase of the slope efficiency for sample S300, while the internal loss of S150 even increases slightly compared to that of S300, which is due to more light penetration into the ITO layer as p-AlGaN thickness reduces. The simulation also shows the internal loss of S500 is 9.8 cm^{-1}, a little lower than that of C500, which may be the cause of the reduced threshold current density for S500.

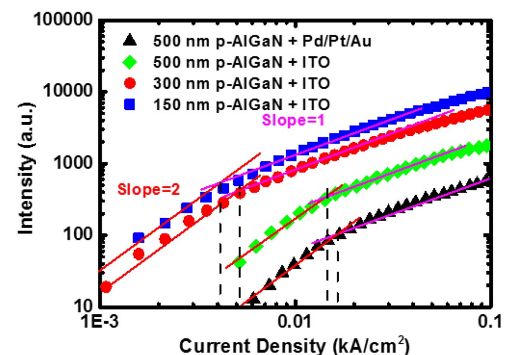

Fig. 4. Integrated electroluminescence intensity as a function of current density in a double logarithmic plot. The intersections of the linear fitting with slopes of 2 and 1 are marked by the dotted lines.

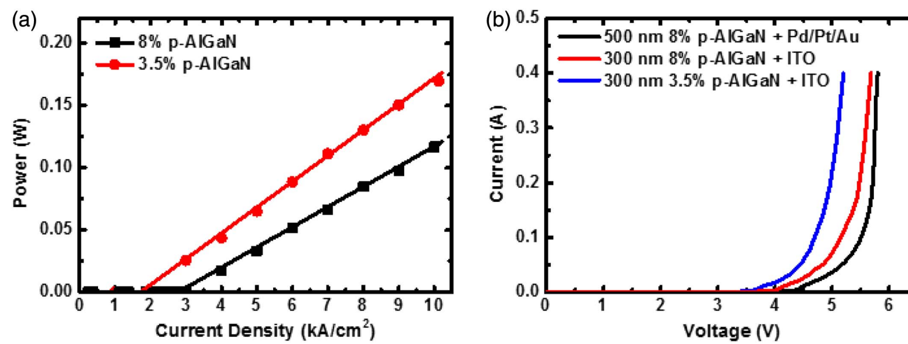

Fig. 5. (a) *P–I* curves of ITO LDs with 300 nm different p-AlGaN cladding layers; Al contents are shown in the legends. (b) *I–V* curves of three different kinds of LDs.

Since Mg activation energy is proportional to Al content in AlGaN:Mg [42], and the concentration of carbon that acts as a compensating donor in AlGaN:Mg [43] decreases with Al content in AlGaN:Mg [44], reducing the Al content of the p-AlGaN cladding layer will lead to increasing hole concentration, meaning increasing hole injection into the active region. Our simulation shows that employing ITO as the cladding layer allows us to decrease the p-AlGaN composition to 3.5% with a negligible increase of internal loss when the thickness is 300 nm. Therefore, we fabricated an ITO LD with a 300 nm p-$Al_{0.035}Ga_{0.965}N$ cladding layer. Figure 5(a) shows the *P–I* curves of ITO LDs with p-AlGaN compositions of 8% and 3.5%, respectively. It can be seen that the threshold current density of ITO LDs with the p-$Al_{0.035}GaN$ cladding layer is 1.6 kA/cm^2, which is 1.3 kA/cm^2 lower than that of ITO LDs with the p-$Al_{0.08}GaN$ cladding layer. The slope efficiency of ITO LDs with the p-$Al_{0.035}GaN$ cladding layer also slightly increases to 0.2 W/A. The improvement of ITO LDs with the p-$Al_{0.035}GaN$ cladding layer is attributed to increasing hole concentration and injection efficiency. Figure 5(b) shows a comparison of the current–voltage (*I–V*) curves of these two LDs and the 500 nm conventional LD under continuous-wave electrical injection. With a decrease of p-AlGaN cladding layer thickness and Al content, the operation voltages of LDs decrease. The operation voltage of the ITO LD with the 300 nm p-$Al_{0.035}GaN$ cladding layer is 0.6 V lower than that of the conventional LD at the current density of 4 kA/cm^2, which is attributed to the reduced series resistance due to reduced thickness and Al content of the p-AlGaN cladding layer.

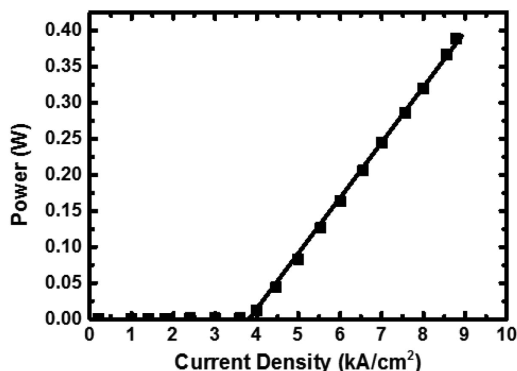

Fig. 6. *P–I* curve of ITO LDs with 300 nm p-$Al_{0.035}GaN$ cladding layer. The front facet coating reflectivity is 40%.

The threshold current density of ITO LD with the p-$Al_{0.035}GaN$ cladding layer is as low as 1.6 kA/cm^2, which allows us to reduce the front facet coating reflectivity to 40% and increase the ridge size to 15 μm wide and 1200 μm long. The *P–I* curve of the ITO LDs is measured under pulse operation and is shown in Fig. 6. The threshold current density is 3.9 kA/cm^2 and the slope efficiency is 0.44 W/A. The output power is as high as 400 mW at the typical current density of 9 kA/cm^2 for GaN-based green LDs.

4. CONCLUSION

In conclusion, simulation shows that the hybrid green LD structure using ITO as the cladding layer enables reducing p-AlGaN cladding layer thickness and composition without increasing the internal loss compared to the conventional LD structure. Green LDs with an ITO cladding layer were then fabricated and characterized. It is found that the threshold current density is reduced greatly from 5 kA/cm^2 to 1.6 kA/cm^2. Moreover, the slope efficiency is increased by 25% and the operation voltage is reduced by 0.6 V for hybrid green LDs. As a result, a 400 mW high-power green LD has been obtained. By reducing the absorption coefficient of ITO further and improving the contact resistivity between ITO and LD structures, the performance of green LDs can be improved further. These results indicate that the hybrid LD structure can pave the way toward high-performance green LDs for laser display application.

Funding. National Key Research and Development Program of China (2016YFB0401803, 2017YFE0131500, 2017YFB0405000); National Natural Science Foundation of China (61834008, 61574160, 61804164, 61704184); Natural Science Foundation of Jiangsu province (BK20180254); China Postdoctoral Science Foundation (2018M630619).

Acknowledgment. We are thankful for the technical support from Nano Fabrication Facility, Platform for Characterization & Test, and Nano-X of SINANO, CAS.

Disclosures. The authors declare no conflicts of interest.

REFERENCES

1. S. Nakamura, “The roles of structural imperfections in InGaN-based blue light-emitting diodes and laser diodes,” Science **281**, 956–961 (1998).
2. F. A. Ponce and D. P. Bour, “Nitride-based semiconductors for blue and green light-emitting devices,” Nature **386**, 351–359 (1997).
3. T. Miyoshi, S. Masui, T. Okada, T. Yanamoto, T. Kozaki, S. Nagahama, and T. Mukai, “510–515 nm InGaN-based green laser diodes on *c*-plane GaN substrate,” Appl. Phys. Express **2**, 062201 (2009).
4. U. Strauss, A. Somers, U. Heine, T. Wurm, M. Peter, C. Eichler, S. Gerhard, G. Bruederl, S. Tautz, B. Stojetz, A. Loeffler, and H. Koenig, “GaInN laser diodes from 440 to 530 nm: a performance study on single mode and multi-mode R&D designs,” Proc. SPIE **10123**, 101230A (2017).
5. S. Takagi, Y. Enya, T. Kyono, M. Adachi, Y. Yoshizumi, T. Sumitomo, Y. Yamanaka, T. Kumano, S. Tokuyama, K. Sumiyoshi, N. Saga, M. Ueno, K. Katayama, T. Ikegami, T. Nakamura, K. Yanashima, H. Nakajima, K. Tasai, K. Naganuma, N. Fuutagawa, Y. Takiguchi, T. Hamaguchi, and M. Ikeda, “High-power (over 100 mW) green laser diodes on semipolar {2021} GaN substrates operating at wavelengths beyond 530 nm,” Appl. Phys. Express **5**, 082102 (2012).
6. S. P. DenBaars, D. Feezell, K. Kelchner, S. Pimputkar, C. C. Pan, C. C. Yen, S. Tanaka, Y. Zhao, N. Pfaff, R. Farrell, M. Iza, S. Keller, U. Mishra, J. S. Speck, and S. Nakamura, “Development of gallium-nitride-based light-emitting diodes (LEDs) and laser diodes for energy-efficient lighting and displays,” Acta Mater. **61**, 945–951 (2013).
7. A. Avramescu, T. Lermer, J. Müller, S. Tautz, D. Queren, S. Lutgen, and U. Strauß, “InGaN laser diodes with 50 mW output power emitting at 515 nm,” Appl. Phys. Lett. **95**, 071103 (2009).
8. J. P. Liu, L. Q. Zhang, D. Y. Li, K. Zhou, Y. Cheng, W. Zhou, A. Q. Tian, M. Ikeda, S. M. Zhang, and H. Yang, “GaN-based blue laser diodes with 2.2 W of light output power under continuous-wave operation,” IEEE Photonics Technol. Lett. **29**, 2203–2206 (2017).
9. A. Q. Tian, J. P. Liu, L. Q. Zhang, Z. C. Li, M. Ikeda, S. M. Zhang, D. Y. Li, P. Y. Wen, F. Zhang, Y. Cheng, X. W. Fan, and H. Yang, “Green laser diodes with low threshold current density via interface engineering of InGaN/GaN quantum well active region,” Opt. Express **25**, 415–421 (2017).
10. Y. Sun, K. Zhou, M. X. Feng, Z. C. Li, Y. Zhou, Q. Sun, J. P. Liu, L. Q. Zhang, D. Y. Li, X. J. Sun, D. B. Li, S. M. Zhang, M. Ikeda, and H. Yang, “Room-temperature continuous-wave electrically pumped InGaN/GaN quantum well blue laser diode directly grown on Si,” Light Sci. Appl. **7**, 13 (2018).
11. A. Q. Tian, J. P. Liu, L. Q. Zhang, L. R. Jiang, M. Ikeda, S. M. Zhang, D. Y. Li, P. Y. Wen, Y. Cheng, X. W. Fan, and H. Yang, “Significant increase of quantum efficiency of green InGaN quantum well by realizing step-flow growth,” Appl. Phys. Lett. **111**, 112102 (2017).
12. L. R. Jiang, J. P. Liu, A. Q. Tian, Y. Cheng, Z. C. Li, L. Q. Zhang, S. M. Zhang, D. Y. Li, M. Ikeda, and H. Yang, “GaN-based green laser diodes,” J. Semicond. **37**, 111001 (2016).
13. J. J. Wierer, J. Y. Tsao, and D. S. Sizov, “Comparison between blue lasers and light-emitting diodes for future solid-state lighting,” Laser Photonics Rev. **7**, 963–993 (2013).
14. Y. Shimada, Y. Chida, N. Ohtsubo, T. Aoki, M. Takeuchi, T. Kuga, and Y. Torii, “A simplified 461-nm laser system using blue laser diodes and a hollow cathode lamp for laser cooling of Sr,” Rev. Sci. Instrum. **84**, 063101 (2013).
15. P. H. Moriya, M. O. Araújo, F. Todão, M. Hemmerling, H. Keßler, R. F. Shiozaki, R. C. Teixerira, and P. W. Courteille, “Comparison between 403 nm and 497 nm repumping schemes for strontium magneto-optical traps,” J. Phys. Commun. **2**, 125008 (2018).
16. S. Fujita, “Wide-bandgap semiconductor materials: for their full bloom,” Jpn. J. Appl. Phys. **54**, 030101 (2015).
17. M. A. Haase, J. Qiu, J. M. DePuydt, and H. Cheng, “Blue-green laser diodes,” Appl. Phys. Lett. **59**, 1272–1274 (1991).
18. Y. Mei, G. E. Weng, B. P. Zhang, J. P. Liu, W. Hofmann, L. Y. Ying, J. Y. Zhang, Z. C. Li, H. Yang, and H. C. Kuo, “Quantum dot vertical-cavity surface-emitting lasers covering the ‘green gap’,” Light Sci. Appl. **6**, e16199 (2016).
19. R. B. Xu, Y. Mei, H. Xu, L. Y. Ying, Z. Zheng, H. Long, D. Zhang, B. P. Zhang, and J. P. Liu, “Green vertical-cavity surface-emitting lasers based on combination of blue-emitting quantum wells and cavity-enhanced recombination,” IEEE Trans. Electron Devices **65**, 4401–4406 (2018).
20. C. P. Massabuau, M. J. Davies, F. Oehler, S. K. Pamenter, E. J. Thrush, M. J. Kappers, A. Kovács, T. Williams, M. A. Hopkins, C. J. Humphreys, P. Dawson, R. E. Dunin-Borkowski, J. Etheridge, D. W. E. Allsopp, and R. A. Oliver, “The impact of trench defects in InGaN/GaN light emitting diodes and implications for the “green gap” problem,” Appl. Phys. Lett. **105**, 112110 (2014).
21. U. Strauß, A. Avramescu, T. Lermer, D. Queren, A. Gomez-Iglesias, C. Eichler, J. Muller, G. Brüderl, and S. Lutgen, “Pros and cons of green InGaN laser on c-plane GaN,” Phys. Status Solidi B **248**, 652–657 (2011).
22. S. Nagahama, T. Yanamoto, M. Sano, and T. Mukai, “Wavelength dependence of InGaN laser diode characteristics,” Jpn. J. Appl. Phys. **40**, 3075–3081 (2001).
23. D. Queren, A. Avramescu, M. Schillgalies, M. Peter, T. Meyer, G. Brüderl, S. Lutgen, and U. Strauß, “Epitaxial design of 475 nm InGaN laser diodes with reduced wavelength shift,” Phys. Status Solidi C **6**, S826–S829 (2009).
24. Z. C. Li, J. P. Liu, M. X. Feng, K. Zhou, S. M. Zhang, H. Wang, D. Y. Li, L. Q. Zhang, D. G. Zhao, D. S. Jiang, H. B. Wang, and H. Yang, “Suppression of thermal degradation of InGaN/GaN quantum wells in green laser diode structures during the epitaxial growth,” Appl. Phys. Lett. **103**, 152109 (2013).
25. J. P. Liu, Z. C. Li, L. Q. Zhang, F. Zhang, A. Q. Tian, K. Zhou, D. Y. Li, S. M. Zhang, and H. Yang, “Realization of InGaN laser diodes above 500 nm by growth optimization of the InGaN/GaN active region,” Appl. Phys. Express **7**, 111001 (2014).
26. D. Bour, C. Chua, Z. H. Yang, M. Teepe, and N. Johnson, “Silver-clad nitride semiconductor laser diode,” Appl. Phys. Lett. **94**, 041124 (2009).
27. T. Margalith, O. Buchinsky, D. A. Cohen, A. C. Abare, M. Hansen, S. P. DenBaars, and L. A. Coldren, “Indium tin oxide contacts to gallium nitride optoelectronic devices,” Appl. Phys. Lett. **74**, 3930–3932 (1999).
28. H. Y. Liu, V. Avrutin, N. Izyumskaya, Ü. Özgür, and H. Morkoç, “Transparent conducting oxides for electrode applications in light emitting and absorbing devices,” Superlattices Microstruct. **48**, 458–484 (2010).
29. A. Myzaferi, A. H. Reading, D. A. Cohen, M. Farrell, S. Nakamura, J. S. Speck, and S. P. DenBaars, “Transparent conducting oxide clad limited area epitaxy semipolar III-nitride laser diodes,” Appl. Phys. Lett. **109**, 061109 (2016).
30. S. Mehari, D. A. Cohen, D. L. Becerra, S. Nakamura, and S. P. Dnbaars, “Demonstration of enhanced continuous-wave operation of blue laser diodes on a semipolar 2021 GaN substrate using indium-tin-oxide/thin-p-GaN cladding layers,” Opt. Express **26**, 1564–1572 (2018).
31. J. Chilwell and I. Hodgkinson, “Thin-films field-transfer matrix theory of planar multilayer waveguides and reflection from prism-loaded waveguides,” J. Opt. Soc. Am. A **1**, 742–753 (1984).
32. G. M. Laws, E. C. Larkins, I. Harrison, C. Molloy, and D. Somerford, “Improved refractive index formulas for the $Al_xGa_{1-x}N$ and $In_yGa_{1-y}N$ alloys,” J. Appl. Phys. **89**, 1108–1115 (2001).
33. L. Q. Zhang, D. S. Jiang, J. J. Zhu, D. G. Zhao, Z. S. Liu, S. M. Zhang, and H. Yang, “Confinement factor and absorption loss of AlInGaN based laser diodes emitting from ultraviolet to green,” J. Appl. Phys. **105**, 023104 (2009).
34. M. Kuc, Ł. Piskorski, A. K. Sokół, M. Dems, M. Wasiak, R. P. Sarzała, and T. Czyszanowski, “Optical simulations of blue and green semipolar InGaN/GaN lasers,” Proc. SPIE **10532**, 1053228 (2019).
35. S. Boycheva, A. K. Sytchkova, and A. Piegari, “Optical and electrical characterization of r.f. sputtered ITO films developed as art protection coatings,” Thin Solid Films **515**, 8474–8478 (2007).
36. A. J. Wen, K. L. Chen, M. H. Yang, W. T. Hsiao, L. G. Chao, and M. S. Leu, “Effect of substrate angle on properties of ITO films deposited by cathodic arc ion plating with In-Sn alloy target,” Surf. Coat. Technol. **198**, 362–366 (2005).

37. M. T. Hardy, C. O. Holder, D. F. Feezell, S. Nakamura, J. S. Speck, D. A. Cohen, and S. P. DenBaars, "Indium-tin-oxide clad blue and true green semipolar InGaN/GaN laser diodes," Appl. Phys. Lett. **103**, 081103 (2013).
38. J. L. Chen and W. D. Brewer, "Ohmic contacts on p-GaN," Adv. Electron. Mater. **1**, 1500113 (2015).
39. J. S. Jang and T. Y. Seong, "Low-resistance and thermally stable indium tin oxide ohmic contacts on strained p-$In_{0.15}Ga_{0.85}N$/p-GaN layer," J. Appl. Phys. **101**, 013711 (2007).
40. M. Meneghini, N. Trivellin, G. Meneghesso, E. Zanoni, U. Zehnder, and B. Hahn, "A combined electro-optical method for the determination of the recombination parameters in InGaN-based light-emitting diodes," J. Appl. Phys. **106**, 114508 (2009).
41. D. Queren, M. Schillgalies, A. Avramescu, G. Brüderl, A. Laubsch, S. Lutgen, and U. Strauß, "Quality and thermal stability of thin InGaN films," J. Cryst. Growth **311**, 2933–2936 (2009).
42. J. Li, T. N. Oder, M. L. Nakarmi, J. Y. Lin, and H. X. Jiang, "Optical and electrical properties of Mg-doped p-type $Al_xGa_{1-x}N$," Appl. Phys. Lett. **80**, 1210–1212 (2002).
43. A. Q. Tian, J. P. Liu, M. Ikeda, S. M. Zhang, Z. C. Li, M. X. Feng, K. Zhou, D. Y. Li, L. Q. Zhang, P. Y. Wen, F. Zhang, and H. Yang, "Conductivity enhancement in AlGaN:Mg by suppressing the incorporation of carbon impurity," Appl. Phys. Express **8**, 051001 (2015).
44. G. Parish, S. Keller, S. P. Denbaars, and U. K. Mishra, "SIMS investigations into the effect of growth conditions on residual impurity and silicon incorporation in GaN and $Al_xGa_{1-x}N$," J. Electron. Mater. **29**, 15–20 (2000).